Petrography and geochemistry of Jumara Dome sediments, Kachchh Basin: Implications for provenance, tectonic setting and weathering intensity

Ahmad A.H.M.[1], Noufal K.N.[1], Masroor Alam M.[2*], and Tavheed Khan[1]

[1] Department of Geology, AMU, Aligarh, India

[2] Department of civil Engineering, ZH College of Engineering and Technology, AMU, Aligarh, India

[*] Corresponding author, E-mail: ahmahmad2004@yahoo.com

Abstract   In the Kachchh Mainland, the Jumara Dome mixed carbonate-siliciclastic succession is represented by the Jhurio and Patcham formations and siliciclastic-dominating Chari Formation (Bathonian to Oxfordian). The Jumara Dome sediments were deposited during sea-level fluctuating, and were interrupted by storms in the shallow marine environment. The sandstones are generally medium-grained, moderately sorted, subangular to subrounded and of low sphericity. The sandstones are mineralogically mature and mainly composed of quartzarenite and subarkose. The plots of petrofacies in the Qt-F-L, Qm-F-Lt, Qp-Lv-Ls and Qm-P-K ternary diagrams suggest mainly the basement uplift source (craton interior) in rifted continental margin basin setting. The sandstones were cemented by carbonate, iron oxide and silica overgrowth. The Chemical Index of Alteration values (73% sandstone and 81% shale) indicate high weathering conditions in the source area. Overall study suggests that such strong chemical weathering conditions are of unconformity with worldwide humid and warm climates during the Jurassic period. Positive correlations between Al_2O_3 and Fe_2O_3, TiO_2, Na_2O, MgO, K_2O are evident. A high correlation coefficient between Al_2O_3 and K_2O in shale samples suggests that clay minerals control the major oxides. The analogous contents of Si, Al, Ti, LREE and TTE in the shale to PAAS with slightly depleted values of other elements ascribe a PAAS like source (granitic gneiss and minor mafics) to the present study. The petrographic and geochemical data strongly suggest that the studied sandstones/shales were deposited on a passive margin of the stable intracratonic basin.

Key words   provenance; tectonic setting; weathering intensity; Kachchh Basin; Jumara Dome

1 Introduction

The mineralogical and chemical compositions of clastic sedimentary rocks are indicative of several variables such as provenance, climate and tectonism (Bhatia and Crook, 1986; Roser and Korsch, 1986, 1988; Cullers, 1988, 2000; Taylor and Mclennan, 1985; Mclennan and Taylor, 1991; Fedo et al., 1997; Cox et al., 1995; Nesbitt et al., 1997). Basu et al. (1975) used the frequency of different types of quartz grains to infer the type of source rocks. The determination of the tectonic setting of sandstones by using the framework mineral composition was firstly proposed by Crook (1974) and has since undergone considerable refinement (Dickinson and Suczek, 1979; Dickinson et al., 1983; Weltje and Eynatten, 2004). The main assumption behind sandstone provenance studies is that different tectonic settings contain their own rock types, which, when eroded, will produce sandstones with specific composition ranges (Dickinson and Suczek, 1979; Dickinson et al., 1983; Dickinson, 1985).

In geochemical studies of the clastic sedimentary rocks, the major elements, trace elements, rare-earth elements and their elemental ratios are the sensitive indicators of source rocks, paleoclimate, paleoweath-

ering conditions and tectonic setting (Bhatia, 1983; Roser and Korsch, 1986; Mclennan et al., 1993; Cullers, 1988, 2000; Condie, 1993). Geochemistry has proven itself to be a very important tool to study the evolution of depositional environment and basin setting. The present study provides a first-hand detailed report on the geochemistry of sandstones and shales of Jumara Dome in order to evaluate the provenance, paleoclimate, paleoweathering conditions and tectonic setting during their deposition.

2 General geology of the study area

The Kachchh marine Jurassic rocks deposited in an extensive area of Tethys at the northwestern corner of the Indian Plate are particularly well known for their mega fossils. The Mesozoic rocks in the Kachchh Basin range from Middle Jurassic to Lower Cretaceous in age and are exposed extensively in the Kachchh Mainland, Wagad, and on the islands of Pachham, Bela, Khadir and Chorar. The mainland outcrops are exposed as a continuous succession from Bajocian to Albian, and consist of most prominent ridge extending for about 193 km from Jawahar Nagar in the east to Jara in the west. The Mesozoic succession developed due to repeated marine incursions during the Middle Jurassic to Early Cretaceous period and was followed upward by the Katrol Formation yielding ammonites of the Kimmeridgian Age (Fur-

sich et al., 1991). The Kachchh Basin evolved due to sequential rifting and repeated movements along Precambrian tectonic trends, which took place in relation to the Indian Plate northward drift after break of the Gondwanaland in the Late Triassic-Early Jurassic (Norton and Sclator, 1979; Biswas, 1987). Kachchh rifting along the Delhi trend was initiated in the Late Triassic as evidenced by continental rhaetic sediments in the northern part of the basin (Koshal, 1984). During Jurassic time, in the early stages of India's northward drift away from Gondwanaland, the Kachchh rift basin was formed from the subsidence of a block between Nagar Parkar Hills and the southwest extension of Aravalli Range. The first occurrence of marine sediments in the Middle Jurassic (Bajocian) indicates that the graben became a fully marine basin during that time. In Early Cretaceous time the basin was filled up and the sea began to recede (Bardan and Datta, 1987). The Late Cretaceous witnessed extensive regional uplift in the western part of India.

In Kachchh, the Jumara Dome mixed carbonate-siliciclastic succession is represented by the Jhurio and Patcham formations and siliciclastic dominating Chari Formation (Bathonian to Oxfordian) (Fig. 1). The lower part of the Jumara Dome is represented by the Jumara Coral Limestone Member, followed upward by the Echinoderm Packstone Member. Above this spongy Limestone Member are the Grey Shale Member and then the Ridge Sandstone Member and Gypsiferous Shale Member come in order (Fig. 2).
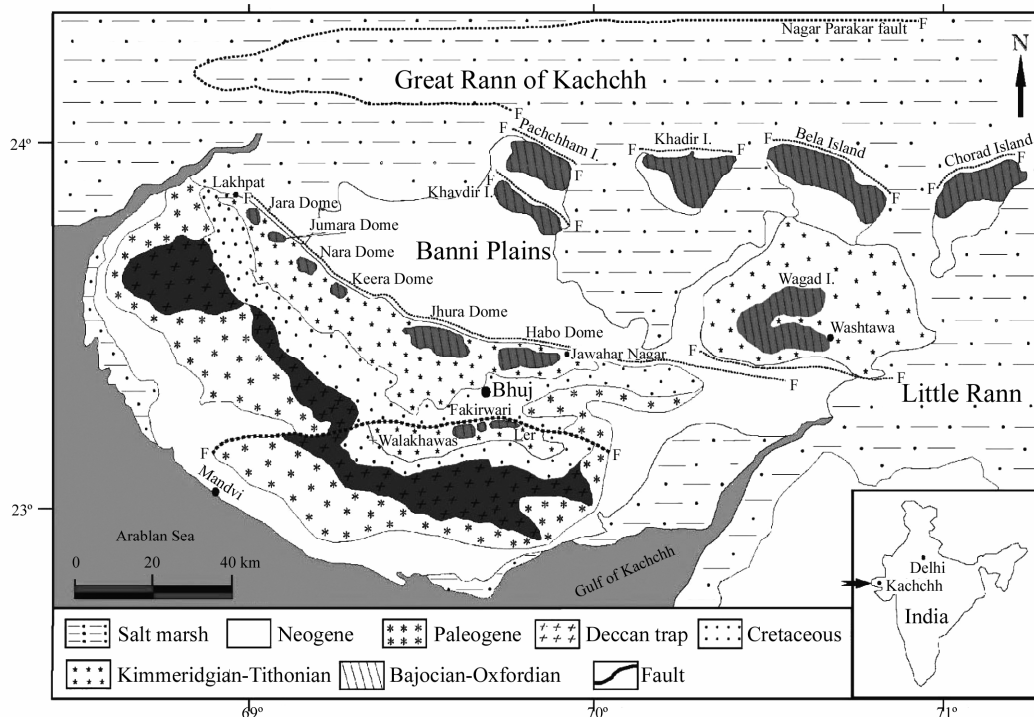
Fig. 1. Geological map of Kachchh Basin showing the study area (after Fursich et al., 2001).
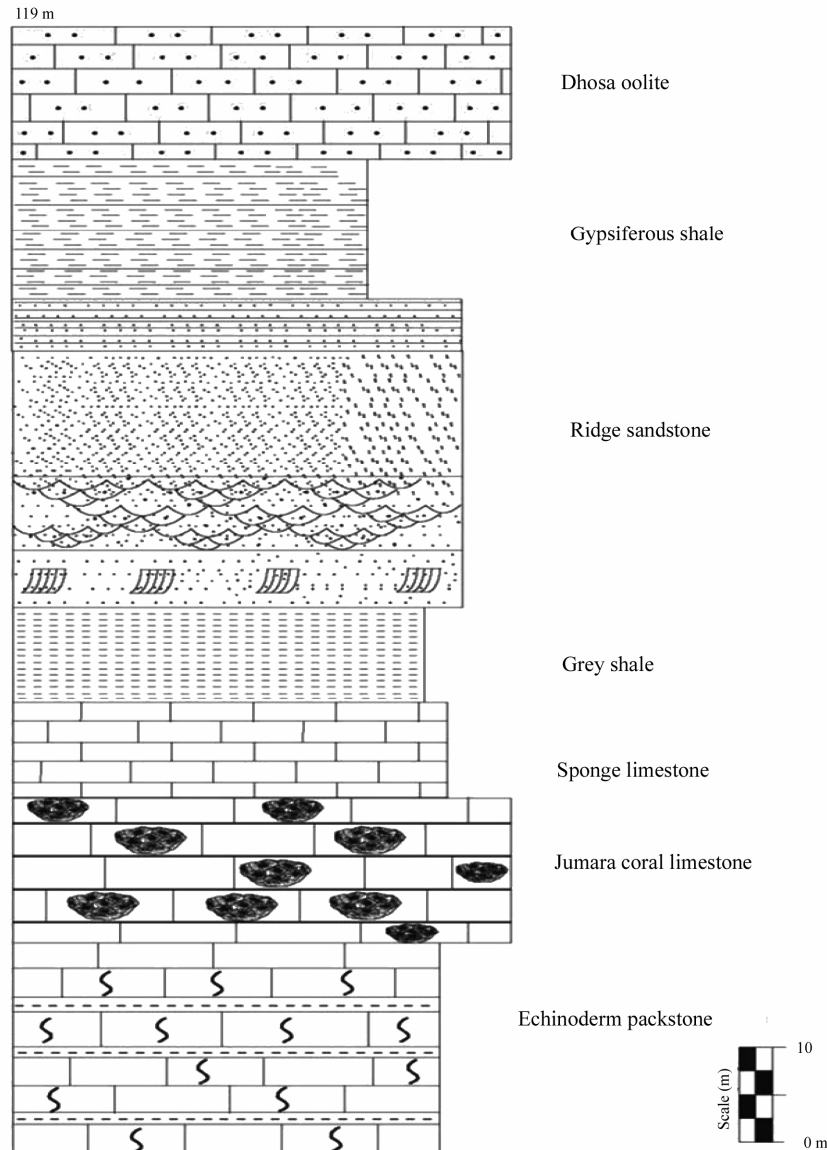
Fig. 2. Measured sections at Jumara.

3 Petrography

The Ridge sandstones are thick- to thin-bedded, reddish-brown, medium- to coarse-grained, moderately to moderately well sorted. The grains are subangular to subrounded with low to medium spherecity. Tabular, trough cross bedding and laminations are common (Plate-IA, B, and C). The sandstones are texturally and compositionally mature. The lower and upper boundaries are sharp and undulating. Scattered quartz pebbles, Thalassonoids and Rhizocorallum are common. The sandstones consist of abundant quartz, followed by feldspar, mica, rock fragments (Plate-IIA) and heavy minerals. The contents follow the order of average percentages of quartz (86.04%), feldspar (8.23%), mica (3.30%), rock fragments (1.94%) and heavy minerals (0.49%). The heavy minerals include opaques, tourmaline, zircon (Plate-IIB), rutile, garnet, staurolite, kyanite, apatite, hornblende and epidote. All the samples of the studied sandstones are plotted near the Q pole in the quartzarenite and subarkose fields.

The shales are grey to bluish, often splintery and brittle micaceous ones. They have alternating thin bands of purplish, fine-grained, micaceous and fissile sandstones. Thin red nodular weathering and mudstone bands are also common in the shales. The upper shale beds are carbonaceous. Thin laminae of quartz and calcite are commonly seen along the bedding. The shales are thick- and thin-bedded and contain lamlibranches, bivalves, brachiopods and ammonoids.

Four types of cement are found in the Ridge sandstone. Carbonate cement occurs in the form of sparry calcite, microcrystalline calcite and blocky cement. Carbonate has replacive relationship with quartz and feldspar (Plate-IIC) where dissolution varies from

surface etching to pseudomorph after carbonates. Precipitation of microcrystalline calcite cement took place at shallow depth above the water table. Later during burial, micrite was replaced by sparry calcite in the meteoric water regime along the interface zone of accretion and saturation. The blocky cement generally completely filled the intergranular pores. The meteoric water environment facilitates the precipitation of block-shaped calcite cement.

Iron oxide cement occurs as a dark brown black coating on the detrital quartz and feldspar grains as well as isolated patches and pervasive pore fillings. Thin iron coating on detrital grains is possibly inherited from source rocks and the presence of corroded quartz grains suggests the presence of earlier carbonate cement which was replaced by iron oxide (Plate-IID). Coating of iron oxide on detrital grains may also be extrabasinal-weathering rinds generated during deep burial (Walker, 1984). Patchy distribution of iron oxide suggests either aborted cementation or dissolution during uplift. Quartz overgrowths are scarce in the Ridge Sandstone (Plate-IIE). The absence of silica cement can be attributed to limited compaction of sandstone, thereby causing very little pressure solution, which is the most important indigenous source of silica. The possible cause for the quartz overgrowth present in these sandstones may be the intraformational release of silica during replacement and corrosion of feldspar and micas by calcite. The authigenic clay occurs as replacement of detrital feldspar and sometimes forms patches within calcite cement. Pseudohexagonal kaolinite and mixed layer of illite and smectite are found within the studied sandstones (Plate-IIF).

The high percentage of floating grains and point contact are mainly found in sandstones with the pervasive development of calcite and Fe-calcite cement, which are probably precipitated at a very early stage. The petrographic study also reveals the presence of several other diagenetic features such as corrosion, oversized pores and complete replacement of detrital grains by carbonate cement. McBride (1985) suggested that the dissolution of feldspar can take place in the shallow weathering zone or during deep burial where it changes into illite and kaolinite.

4 Methods

The study is based on the measurement of a stratigraphic section. For petrographic and geochemical analysis, samples were collected at 50 cm intervals to represent the total thickness of the measured section. Out of the collected sandstone samples, 25 samples were studied petrographically after etching and staining for calcite potash feldspar and pore spaces. For Qt-F-L and Qm-F-Lt plots, the detrital modes were recalculated to 100 percent by summing up Qt, Qm, F, L and Lt framework constituents following Dickinson (1985).

Twenty-one representative samples (16 sandstone samples and 5 shale samples) have been selected for their geochemical analysis. The major, trace and LREE elements of such selected samples were analyzed by XRF (S4 pioneer-Bruker) systems at CESS (Centre for Earth Science Studies), Thiruvananthapuram.

5 Sandstone petrofacies

To understand the tectonic setting of the studied sandstones, the petrofacies are plotted in standard triangular diagrams Qt-F-L, Qm-F-Lt, Qp-Lv-Ls and Qm-P-K given by Dickinson (1985) (Table 1). In the Qt-F-L plot, where all quartz grains are plotted together, the emphasis is put on grain stability and then on weathering, provenance, relief and transport mechanism as well as source rocks, while in Qm-F-Lt, where all lithic fragments are plotted together, the emphasis is shifted towards the grain size of source rocks, because fine-grained rocks yield more lithic fragments in the sand-size range. On the Qt-F-L diagram mean detrital modes plot near Qt pole and Qt-F leg, thereby suggesting a stable, mature craton interior block provenance (Fig. 3A). A population shift towards the Qm-F-Lt and F-Lt legs is evident in the Qm-F-Lt diagram. This diagram shows that the plot of the data falls in continental block provenance with a small amount of contribution from recycled orogenic provenance (Fig. 3B). The Qp-Lv-Ls plot, which is based on rock fragment population from a polygenetic source, gives a more resolved picture about the tectonic elements. The sample data fall in the continental margin, collision suture and fold thrust belt (Fig. 3C). The Qm-P-K plot of the data shows that all the sediment contribution is from the continental basement uplift provenance and reflects mineralogical maturity of the sediments (Fig. 3D). The sandstone petrofacies and heavy mineral suites of the Ridge sandstone indicate multiple rock sources for these sandstones, which are not shown in the triangular plots. The apparent reason for this could be diagenetic alteration and weathering of unstable framework grains, which increased the proportion of quartz grains relative to the original detrital composition.

6 Geochemistry

As seen in Table 2, SiO_2 concentrations show an average of 73.87% within sandstone samples and 62.85% within shale samples; Al_2O_3, 10.46% in sandstones, 21.56% in shales; TiO_2 and K_2O, 0.45% in sandstones, 1.18% in shales; and 0.45% in sandstones,
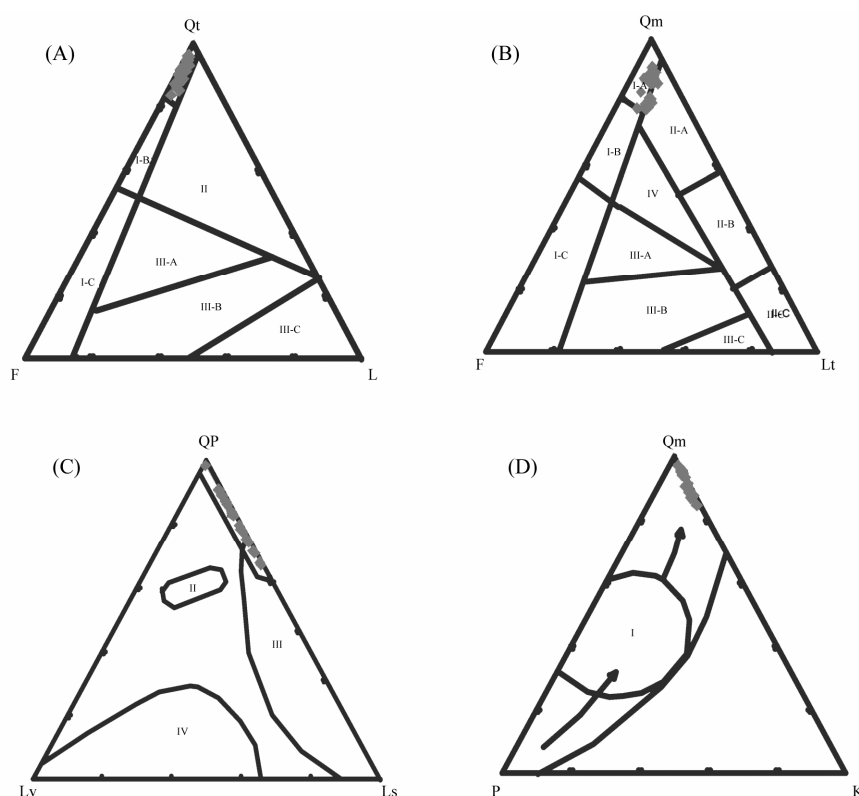
Fig. 3. Tectono-provenance discrimination diagrams (Dickinson, 1985) for Ridge sandstone.

Table 1   Percentage of framework modes of the Ridge sandstone of Jumara Dome, Kachchh, Gujarat
(based on classification of Dickinson, 1985)

SI. No.	Qt	F	L	Qm	F	Lt	Qp	Lv	Ls	Qm	P	K
R1	94.82	4.29	0.89	91.32	4.29	4.38	79.81	0.00	20.19	95.51	0.81	3.68
R3	86.28	11.86	1.87	83.08	11.86	5.07	72.06	0.00	27.94	87.51	1.80	10.68
R4	85.87	12.07	2.06	78.22	12.07	9.71	78.80	0.00	21.20	86.63	1.24	12.13
R8	83.82	12.46	3.72	79.39	12.46	8.15	85.31	0.00	14.69	86.44	0.93	12.63
R9	94.61	4.69	0.70	90.93	4.69	4.38	84.01	0.00	15.99	95.10	0.53	4.38
R10	89.73	7.57	2.70	85.95	7.57	6.48	68.42	0.00	31.58	91.91	0.71	7.38
R11	90.16	9.26	0.59	87.27	8.96	3.76	84.93	0.00	15.07	90.69	0.74	8.57
R12	84.10	12.74	3.16	78.37	12.74	8.89	81.12	0.00	18.88	86.02	1.41	12.58
R13	82.38	15.60	2.02	77.90	15.60	6.50	68.98	0.00	31.02	83.31	1.52	15.17
R14	91.90	5.88	2.22	86.88	5.88	7.23	100.00	0.00	0.00	93.66	0.84	5.50
R15	91.78	5.51	2.71	87.79	5.51	6.71	100.00	0.00	0.00	94.10	0.56	5.34
R16	84.46	12.88	2.67	78.38	12.88	8.74	87.71	0.00	12.29	85.89	1.62	12.49
R17	92.05	6.51	1.44	88.80	6.51	4.68	100.00	0.00	0.00	93.17	0.69	6.14
R18	91.92	6.69	1.39	85.91	6.69	7.39	92.50	0.00	7.50	92.77	0.96	6.27
R19	93.20	5.35	1.45	85.74	5.35	8.91	90.94	0.00	9.06	94.13	0.20	5.67
R20	85.81	12.91	1.28	77.64	12.91	9.45	92.42	0.00	7.58	85.74	2.15	12.11
R21	87.33	9.68	2.99	81.02	9.68	9.30	88.76	0.00	11.24	89.33	2.12	8.56
R22	92.80	5.62	1.59	86.54	5.62	7.84	100.00	0.00	0.00	93.91	0.85	5.25
R23	86.17	10.05	3.78	79.66	10.15	10.19	90.61	0.00	9.39	88.70	1.56	9.74
R24	93.33	5.78	0.89	86.64	5.78	7.58	100.00	0.00	0.00	93.75	0.53	5.72
R25	85.97	9.95	4.08	81.47	9.95	8.57	75.58	0.00	24.42	89.12	0.99	9.90
R26	91.45	7.13	1.41	86.00	7.13	6.87	79.42	0.00	20.58	92.34	0.52	7.14
R27	87.66	10.31	2.03	81.32	10.31	8.37	90.33	0.00	9.67	88.75	1.59	9.66
R28	93.25	5.04	1.71	88.64	5.04	6.32	72.92	0.00	27.08	94.62	0.90	4.48
R30	93.56	4.39	2.05	89.20	4.39	6.41	76.62	0.00	23.38	95.31	0.75	3.94
Average	89.38	8.57	2.05	84.16	8.56	7.28	85.65	0.00	14.35	90.74	1.06	8.20

Table 2   Major and trace element abundance of Ridge sandstone and Grey shale of Jumara Dome, Kachchh Gujarat (Oxides in wt.%) (trace elements in ×10⁻⁶)

Elements	Ridge sandstone																Grey shale				
	R-3	R-8	R-9	R-10	R-11	R-15	R-16	R-18	R-21	R-22	R-23	R-24	R-25	R-26	R-27	R-28	B-1	B-2	B-3	G-1	G2
SiO_2	75.84	75.66	73.82	75.00	68.07	71.22	70.51	67.11	69.46	64.64	79.13	75.59	78.74	74.35	83.12	77.81	59.71	62.31	69.22	61.77	60.66
TiO_2	0.59	0.31	0.34	0.35	0.39	0.43	0.49	0.40	0.42	0.24	0.53	0.62	0.42	0.62	0.47	0.62	1.21	1.2	0.94	1.34	1.21
Al_2O_3	14.49	8.08	9.56	7.89	9.77	9.79	12.08	9.65	10.46	9.27	11.54	11.44	9.27	10.78	10.04	13.01	24.37	23.3	20.13	20.57	19.22
MnO	0.01	0.02	0.04	0.08	0.10	0.04	0.18	0.08	0.09	0.12	0.02	0.09	0.11	0.06	0.02	0.01	0	0	0.01	0.02	0.02
Fe_2O_3	2.28	0.60	0.94	3.32	1.03	1.19	1.99	1.06	1.20	0.89	3.39	2.52	1.96	1.91	2.16	2.6	1.85	1.55	2.28	8.01	6.84
CaO	0.39	7.75	8.50	4.89	14.11	9.21	2.82	11.82	9.38	14.28	0.44	2.69	3.8	3.44	0.18	0.81	0.23	0.29	0.34	0.2	0.8
MgO	0.47	0.24	0.17	2.11	0.22	0.14	0.72	0.25	0.15	0.08	0.15	1.00	0.02	1.76	0.08	0.15	0.92	0.79	0.86	2.37	2.31
Na_2O	0.63	0.32	0.36	0.34	0.41	0.45	0.61	0.43	0.57	0.45	0.52	0.41	0.44	0.51	0.46	0.57	0.48	0.34	0.61	1.48	1.35
K_2O	1.90	1.25	1.44	1.32	1.60	1.63	1.92	1.60	1.86	1.73	1.62	1.56	1.42	1.65	1.45	1.92	2.46	2.46	2.67	2.53	2.39
P_2O_5	0.05	0.10	0.13	0.10	0.10	0.09	0.07	0.08	0.09	0.04	0.12	0.06	0.1	0.08	0.1	0.14	0.07	0.06	0.06	0.07	0.06
LOI	3.12	5.51	4.58	4.41	4.02	5.65	8.42	7.35	6.17	8.13	2.35	3.84	3.6	4.69	1.76	2.19	8.44	7.48	2.67	1.48	4.99
CIA	79.33	81.24	81.74	79.99	80.35	79.75	59.59	79.94	78.14	78.13	77.30	61.22	50.29	54.86	79.21	74.44	86.35	86.17	81.77	79.00	75.60
PIA	87.88	92.95	93.31	92.26	92.48	91.79	62.07	92.03	90.28	91.16	85.72	63.71	50.35	55.95	88.86	82.09	94.83	95.07	91.55	86.75	82.17
CIW	89.42	94.06	94.34	93.57	93.73	93.17	66.42	93.37	92.01	92.82	87.62	67.32	54.88	60.36	90.44	84.51	95.37	95.61	92.67	88.31	84.19
ICV	0.50	0.41	0.38	1.27	0.43	0.43	1.01	0.45	0.45	0.41	0.58	1.08	1.20	1.43	0.48	0.56	0.37	0.36	0.46	0.89	0.94
Cr	46	16	20	22	23	26	40	23	27	17	38	44	30	41	32	43	111	106	91	133	127
Co	17	11	8	15	8	9	15	7	11	8	16	15	28	14	17	15	11	10	13	19	17
Ni	33	0	3	11	2	4	37	11	25	3	67	22	62	20	34	71	39	31	28	62	53
Cu	7	0	1	5	1	0	8	2	5	0	8	3	0	0	4	11	72	65	38	27	24
Zn	11	0	13	193	0	18	34	63	22	0	73	48	62	34	37	90	1	0	1	80	73
Ga	13	0	0	3	0	0	5	0	0	0	10	8	6	7	5	12	43	40	32	48	34
Rb	95	65	79	63	73	69	92	55	77	62	73	76	84	82	68	92	174	169	160	159	133
Y	22	15	27	13	27	26	19	37	33	19	29	26	23	22	26	51	42	52	45	28	34
Zr	693	293	310	278	411	434	413	539	459	187	617	631	425	736	580	691	728	859	788	421	560
Nb	9	8	10	8	9	8	10	5	8	6	8	8	11	9	7	10	16	16	13	16	12
Ba	459	294	334	349	322	352	437	341	413	359	405	348	335	360	340	470	470	465	548	213	224
La	27	39	47	33	28	25	28	31	29	16	33	27	28	30	29	34	48	57	37	37	32
Ce	45	74	112	71	44	39	45	46	51	21	67	48	47	61	61	62	82	115	72	82	57
Sm	4	5	5	4	5	4	3	3	4	3	4	4	4	4	4	5	6	5	4	5	5

and 2.5% in shales. Na_2O concentrations have an average of 0.46% within sandstones and 0.85% in shales, while Fe_2O_3, 1.81% in sandstones; CaO, 5.91% in sandstones, 0.37% in shales; P_2O_5 and MnO, 0.09% in sandstones, 0.06% in shales; and 0.07% in sandstones, and 0.01% in shales. The average value of MgO is 0.48% in sandstones and 1.45% in shales).

The concentrations of Rb within sandstones have an average of $75.31×10^{-6}$ and in shales $159×10^{-6}$; Ba, $369.87×10^{-6}$ in sandstones, $384×10^{-6}$ in shales; and Ga, $4.31×10^{-6}$ in sandstones, and $39.4×10^{-6}$ in shales. Cr concentrations in sandstones have an average of $30.5×10^{-6}$ and in shales, $113.6×10^{-6}$; CO, $13.37×10^{-6}$ in sandstones, $14×10^{-6}$ in shales; Ni, $25.31×10^{-6}$ in sandstones, $42.6×10^{-6}$ in shales; Cu, $3.43×10^{-6}$ in sandstones, $45.2×10^{-6}$ in shales; and Zn, $43.62×10^{-6}$ in sandstones, $31×10^{-6}$ in shales. Zr values within sandstones show an average of $481.06×10^{-6}$ and in shales, $671.2×10^{-6}$, while Y and Nb vary over a narrow range. La values within sandstone samples average 32.25

$×10^{-6}$ and in shales, $42.2×10^{-6}$; Sm, $4.06×10^{-6}$ in sandstones, $5×10^{-6}$ in shales; and Ce, $55.87×10^{-6}$ in sandstones, and $81.6×10^{-6}$ in shales.

The correlation matrix indicates certain association in sandstones and shales of Jumara Dome (Table 3). In sandstone samples, Al_2O_3 shows weak positive relationship with SiO_2 ($r=0.20$) and strong positive relationship with K_2O ($r=0.79$) and Na_2O ($r=0.85$), and weak inverse relationship with MgO ($r= -0.09$). A strong positive correlation of Al_2O_3 with TiO_2 ($r=0.79$) and a moderate positive correlation with Fe_2O_3 ($r=0.38$) are observed. Furthermore, there is a moderate positive relationship between MgO and Fe_2O_3 ($r=0.45$). Similarly, K_2O shows moderate positive relationship with Na_2O ($r=0.60$) and TiO_2 ($r=0.46$) (Fig. 4). These relationships suggest the control of clay fraction appears in the sandstones on the major oxide abundance.

In shale samples, Al_2O_3 shows a moderate inverse correlation with SiO_2 ($r=-0.37$) and weak inverse

correlation with K_2O (r= -0.19) along with strong inverse relationship with Na_2O (r= -0.73). Al_2O_3 also shows a moderate inverse correlation with MgO (r= -0.65) and Fe_2O_3 (r= -0.68), and weak positive relationship with TiO_2 (r=0.18). There is a strong positive correlation between MgO and Fe_2O_3 (r=0.99). The alkali oxides K_2O and Na_2O are in weak inverse relationship, while there is strong negative relationship between K_2O and TiO_2 (r= -0.66). The elemental relationship displays by shale samples demonstrate control of source rocks in the provenance. MgO shows weak positive relationship with Cr (r=0.21), weak inverse relationship with Ni (r= -0.17) and moderate positive relationship with Zn (r=0.57) in sandstones. Moderate inverse negative relationship between K_2O and Ba (r= -0.43) and strong positive relationship between K_2O and Rb(r=0.92) are evident. There is a strong positive correlation of Zr with Al_2O_3 (r=0.73), a moderate positive correlation with K_2O(r=0.55) and Y (r=0.50), and strong positive relationship with TiO_2(r=0.93) in sandstones. These relations are generally found in felsic igneous rocks. The weak positive relationship of TTE (Transition Trace Elements) with MgO is probably a sorting effect. In shale samples MgO shows a strong positive correlation with Cr (r=0.89), Ni (r=0.95) and Zn(r=0.99). There is a moderate positive correlation between K_2O and Ba (r=0.52), K_2O and Rb (r=0.31). Zr is moderately positive to Al_2O_3 (r=0.52), strongly positive to Y (r=0.98), weakly positive to K_2O (r=0.20) and moderately inverse with TiO_2 (r= -0.63) (Fig. 5). The relationship suggests that the debris in shales is derived from mafic igneous rocks in which the TTEs are fractionated with MgO.

6.1 Paleoweathering conditions and tectonic setting

The most widely used chemical index to ascertain the degree of source area weathering is the Chemical Index of Alteration (CIA) proposed by Nesbitt and Young (1982) based on the calculation in terms of molecular proportion.

CIA= $[Al_2O_3/(Al_2O_3+CaO^*+Na_2O+K_2O)]\times100$

where CaO^* represents CaO values in silicate fraction only. The CIA values of sandstones and shales of Jumara Dome range from 50.28 to 81.73 (average 73.47), and 75.60 to 86.34 (average 81.77), respectively. Variations in CIA reflect changes in the properties of feldspar versus aluminous clay minerals. These CIA values indicate that the sediments are moderately to highly weathered, which in turn suggests that the sediments have been derived from the source rocks that were subjected to both physical and chemical breakdown.

CIW= $[Al_2O_3/(Al_2O_3+CaO^*+Na_2O)]\times100$
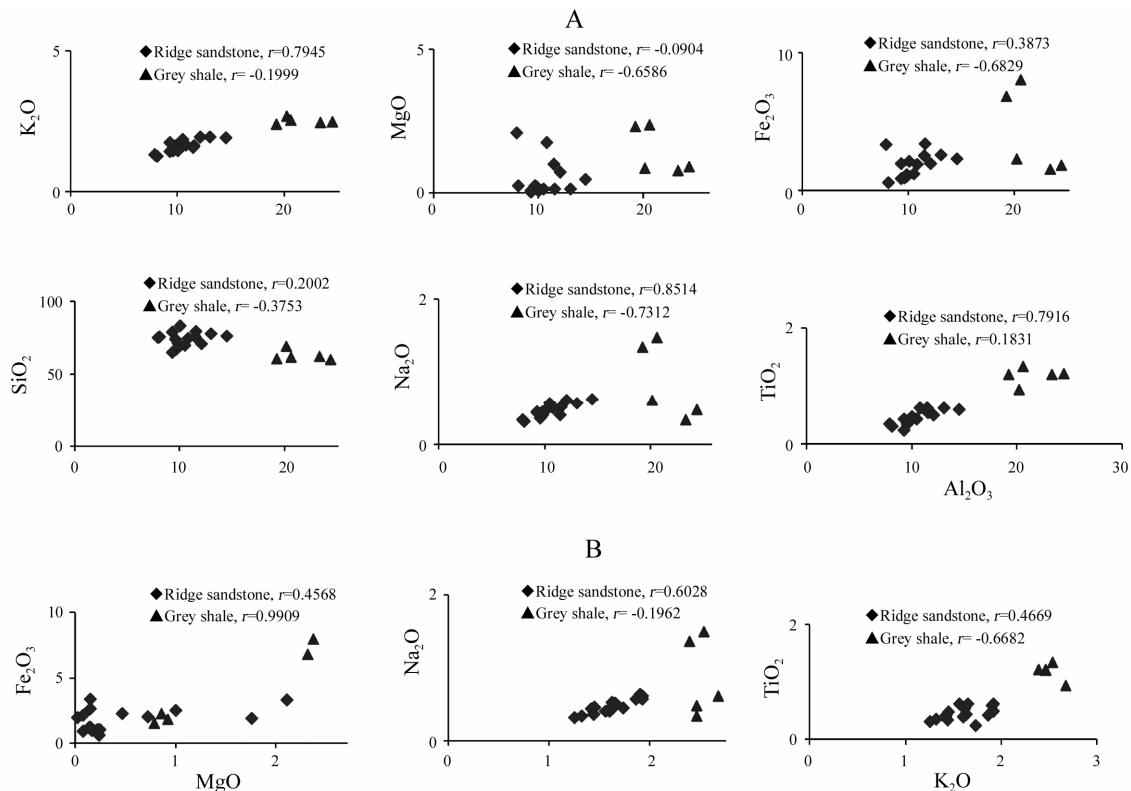
Fig. 4. A. Al_2O_3 versus major oxides covariation diagram. B. Covariation diagram of K_2O versus Na_2O and TiO_2 and MgO versus Fe_2O_3 of Jumara Dome sediments.

Table 3 Correlation coefficient among chemical parameters of Ridge sandstone and Grey Shale, Jumara Dome, Kachchh, Gujarat

A. Ridge sandstone

	SiO_2	TiO_2	Al_2O_3	MnO	Fe_2O_3	CaO	MgO	Na_2O	K_2O	P_2O_5	CIA	Cr	Co	Ni	Rb	Ba	Y	Zr	Nb	La	Sm	Cu	Zn	Ga	Ce
SiO_2	1.00																								
TiO_2	0.47	1.00																							
Al_2O_3	0.20	0.79	1.00																						
MnO	-0.57	-0.26	-0.18	1.00																					
Fe_2O_3	0.61	0.65	0.39	-0.16	1.00																				
CaO	-0.85	-0.74	-0.57	0.36	-0.78	1.00																			
MgO	0.05	0.24	-0.09	0.16	0.46	-0.13	1.00																		
Na_2O	0.03	0.60	0.85	0.06	0.28	-0.24	-0.16	1.00																	
K_2O	-0.30	0.47	0.79	0.18	0.08	-0.43	-0.18	0.91	1.00																
P_2O_5	0.46	0.02	-0.15	-0.45	0.17	-0.12	0.07	-0.21	-0.50	1.00															
CIA	0.78	0.78	0.71	-0.39	0.75	-0.19	0.21	-0.18	0.66	0.12	1.00														
Cr	0.45	0.96	0.71	-0.12	0.64	-0.95	0.09	0.56	0.90	-0.10	0.84	1.00													
Co	0.70	0.40	0.87	0.01	0.59	-0.79	-0.18	0.72	0.02	0.08	0.62	0.50	1.00												
Ni	0.60	0.59	0.23	-0.15	0.66	-0.72	0.00	0.25	0.42	0.34	0.76	0.66	0.73	1.00											
Rb	0.31	0.64	0.77	0.00	0.29	-0.73	-0.03	0.57	0.92	0.07	0.58	0.73	0.73	0.57	1.00										
Ba	0.08	0.58	0.85	-0.06	0.45	-0.58	-0.42	0.69	0.10	-0.04	0.59	0.69	0.49	0.09	0.70	1.00									
Y	0.05	0.40	0.42	-0.30	0.05	-0.07	0.11	0.90	0.55	0.46	0.21	0.29	0.32	0.46	0.20	0.43	1.00								
Zr	0.46	0.94	0.73	-0.41	0.47	-0.64	0.05	0.36	0.79	0.05	0.73	0.85	0.53	0.55	0.47	0.49	0.50	1.00							
Nb	0.37	0.33	0.30	0.05	0.21	-0.41	0.04	0.57	0.40	0.39	0.29	0.37	-0.11	0.43	0.81	0.28	0.50	0.13	1.00						
La	0.36	-0.03	-0.15	-0.43	0.00	-0.17	-0.12	0.23	0.34	0.73	0.03	-0.14	0.32	0.00	0.08	-0.16	0.13	-0.02	0.34	1.00					
Sm	0.38	0.06	-0.06	-0.57	-0.07	-0.07	0.03	-0.34	0.81	0.68	0.69	-0.08	-0.08	0.68	0.21	-0.17	0.21	0.05	0.48	0.63	1.00				
Cu	0.33	0.53	0.69	-0.16	0.66	-0.62	0.57	-0.31	-0.21	0.24	0.22	0.62	-0.03	0.32	0.91	0.85	0.44	0.44	0.21	0.09	-0.01	1.00			
Zn	0.31	0.12	-0.15	-0.01	0.73	-0.36	0.16	0.65	0.89	0.31	0.91	0.11	0.25	0.77	-0.12	0.12	0.04	0.05	0.02	0.16	-0.08	0.40	1.00		
Ga	0.62	0.83	0.79	-0.56	0.75	-0.86	0.14	0.59	0.29	0.04	0.40	0.89	0.34	0.32	0.68	0.67	0.44	0.76	0.38	-0.04	0.06	0.66	0.26	1.00	
Ce	0.44	-0.04	-0.18	-0.45	0.10	-0.24		-0.37		0.70	0.40	-0.13	-0.04	-0.02	0.06	-0.18	0.02	-0.05	0.33	0.95	0.61	0.06	0.20	0.50	1.00

B. Grey shale

	SiO_2	TiO_2	Al_2O_3	MnO	Fe_2O_3	CaO	MgO	Na_2O	K_2O	P_2O_5	CIA	Cr	Co	Ni	Rb	Ba	Y	Zr	Nb	La	Sm	Cu	Zn	Ga	Ce
SiO_2	1.00																								
TiO_2	-0.85	1.00																							
Al_2O_3	-0.38	0.18	1.00																						
MnO	0.02	0.24	-0.89	1.00																					
Fe_2O_3	-0.30	0.57	-0.68	0.93	1.00																				
CaO	-0.13	-0.09	-0.61	0.49	0.36	1.00																			
MgO	-0.38	0.60	-0.66	0.91	0.99	0.45	1.00																		
Na_2O	-0.24	0.49	-0.73	0.96	0.99	0.40	0.99	1.00																	
K_2O	0.90	-0.67	-0.20	-0.01	-0.24	-0.47	-0.36	-0.20	1.00																
P_2O_5	-0.48	0.59	0.40	-0.01	0.24	-0.59	0.21	0.22	-0.06	1.00															
CIA	0.00	-0.15	0.92	-0.97	-0.87	-0.70	-0.87	-0.90	0.13	0.18	1.00														
Cr	-0.72	0.88	-0.26	0.64	0.87	0.25	0.90	0.83	-0.61	0.45	-0.58	1.00													
Co	-0.12	0.42	-0.76	0.97	0.98	0.32	0.95	0.99	-0.05	0.23	-0.89	0.76	1.00												
Ni	-0.55	0.77	-0.41	0.77	0.94	0.21	0.95	0.92	-0.40	0.49	-0.69	0.96	0.89	1.00											
Rb	0.05	-0.04	0.85	-0.81	-0.68	-0.91	-0.73	-0.72	0.31	0.44	0.93	-0.46	-0.67	-0.49	1.00										
Ba	0.55	-0.74	0.51	-0.80	-0.95	-0.42	-0.97	-0.92	0.52	-0.25	0.77	-0.96	-0.87	-0.96	0.66	1.00									
Y	0.33	-0.54	0.55	-0.85	-0.93	-0.21	-0.92	-0.94	0.15	-0.50	0.76	-0.83	-0.94	-0.94	0.52	0.86	1.00								
Zr	0.37	-0.63	0.53	-0.51	-0.96	-0.18	-0.95	-0.96	0.20	-0.49	0.75	-0.88	-0.95	-0.97	0.51	0.91	0.99	1.00							
Nb	-0.38	0.53	0.78	-0.89	-0.23	-0.84	-0.26	-0.31	-0.06	0.66	0.68	0.11	-0.30	0.02	0.82	0.12	0.14	0.07	1.00						
La	-0.20	0.10	0.88	-0.35	-0.05	-0.54	-0.71	-0.79	-0.16	0.03	0.90	-0.36	-0.82	-0.55	0.77	0.54	0.75	0.68	0.71	1.00					
Sm	-0.89	0.66	0.68	-0.98	-0.84	-0.16	0.03	-0.09	-0.69	0.65	0.35	0.42	-0.18	0.27	0.31	-0.18	-0.11	-0.12	0.54	0.38	1.00				
Cu	-0.22	-0.04	0.97	0.91	0.99	0.42	1.00	0.98	-0.13	0.18	0.96	-0.47	-0.90	-0.62	0.82	0.68	0.73	0.72	0.62	0.89	0.55	1.00			
Zn	-0.37	0.60	-0.66			-0.64			-0.34	0.20	-0.87	0.89	0.95	0.95	-0.71	-0.98	-0.91	-0.94	-0.24	-0.69	0.00	-0.81	1.00		
Ga	-0.57	0.81	0.45	-0.04	0.28	-0.64	0.25	0.21	-0.21	0.85	0.24	0.56	0.21	0.52	0.47	-0.36	-0.38	-0.45	0.86	0.30	0.59	0.21	0.27	1.00	
Ce	-0.08	0.19	0.69	-0.68	-0.51	-0.63	-0.54	-0.60	-0.02	0.02	0.76	-0.25	-0.60	-0.40	0.72	0.38	0.62	0.51	0.77	0.92	0.17	0.67	-0.50	0.41	1.00
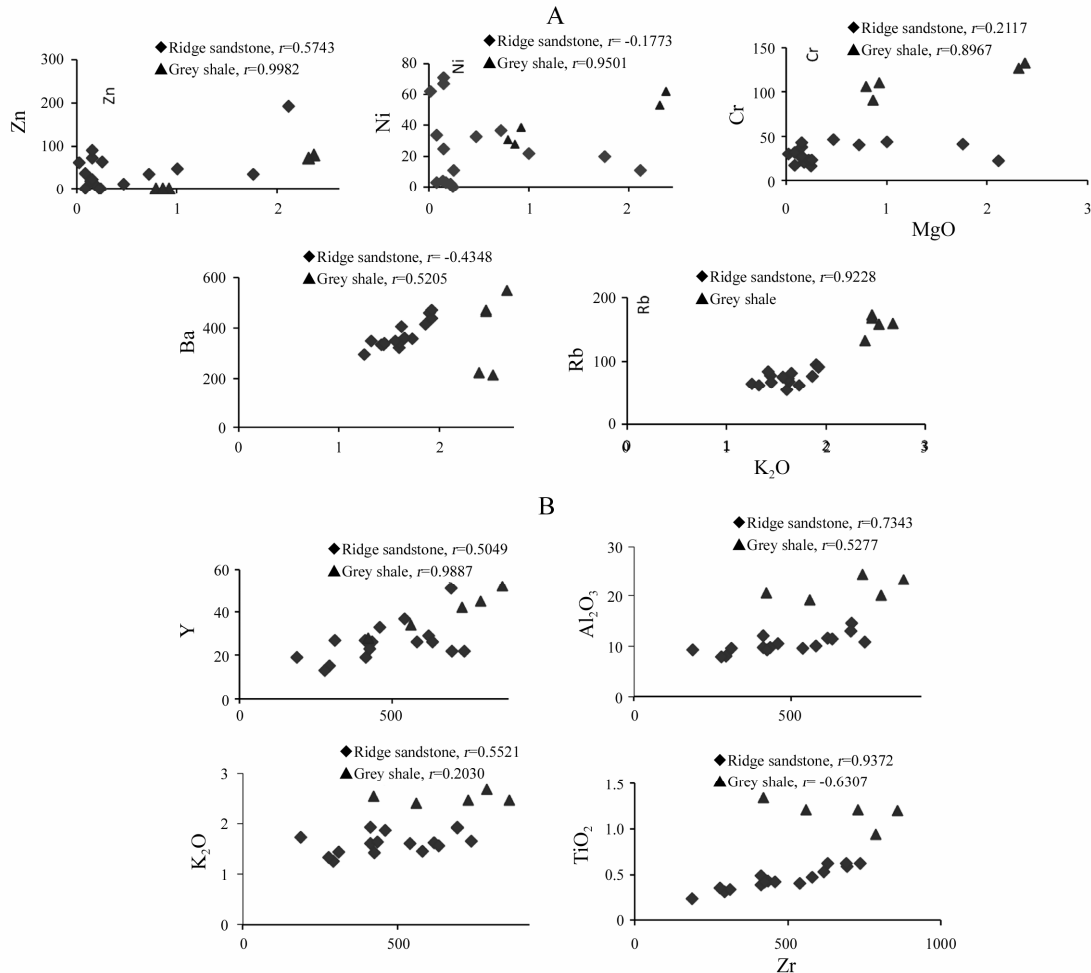
Fig. 5. A. Covariation diagram of K$_2$O versus Rb and Ba and MgO versus Cr, Ni, and Zn of Jumara Dome sediments. B. Covariation diagram of Zr versus TiO$_2$, Al$_2$O$_3$, K$_2$O and Y of Jumara Dome sediments.

CIW index values for the source rocks and sediments reflect the amount of chemical weathering experienced by weathering materials. In comparison to other weathering indices, it is a superior method involving a restricted number of components, which have been simply well known with consistent geochemical behavior during weathering. CIW values of the studied sandstones and shales range from 54.87 to 94.33 (average 84.25), and 84.19 to 95.60 (average 91.23), respectively. CIW indices are higher than CIA values for the analyzed samples due to exclusion of K$_2$O from the index. On the basis of CIW, the studied sediments may be interpreted to show moderate to high weathering.

$$PIA= [(Al_2O_3-K_2O)/(Al_2O_3+CaO^*+Na_2O-K_2O)]\times100$$

The maximum value of PIA is 100 for completely altered materials (kaolinite and gibbsite) and weathered plagioclase has a PIA value of 50. PIA values of the sandstones show large variations from 50.34 to 93.30 (average 82.05) and those of shales vary over a narrow range from 82.16 to 95.06 (average 90.37). PIA values of the sediments further ascribe moderate to intense plagioclase weathering in the source area.

$$ICV= [Fe_2O_3+K_2O+Na_2O+CaO+MgO+MnO+TiO_2]/Al_2O_3]$$

The sandstones/shales with ICV>1 are compositionally immature with the first cycle of sediments deposited in tectonically active settings. On the other hand, those with ICV<1 are compositionally mature and are deposited in the tectonically quiescent or cratonic environment, where sediment recycling is active (Cox et al., 1995). The ICV values for the studied sandstones vary from 0.38 to 1.43 (average 0.69) and shales from 0.35 to 0.93 (average 0.60). On the basis of average ICV values [0.69 (sandstone)-0.60 (shales)], it can be interpreted that both sandstones and shales are compositionally mature and deposited in the tectonically quiescent or cratonic environment.

The A-CN-K plot (Nesbitt and Young, 1984) depicts the clustering of points near the A-K edge, along with illite composition, indicating high extents of weathering of the source rocks. The source rock composition can be determined by backward projection, and parallel to the A-CN line of the weathered sam-

ples to a point on the feldspar join. The clastic rock samples in the present study (Fig. 6) lie along a trend line parallel to A-CN axis emerging from diorite reaching up to the illite stability zone. The source rock is simultaneously subjected to physical and moderately intense chemical weathering to produce debris for these sediments.

6.2 Paleoclimate

Chemical weathering is an important mechanism driving elemental fractionation away from parental bedrock signatures (Nesbitt and Young, 1982). The extent of fractionation depends on bedrock, and local weathering conditions are generally associated with the warm and humid climates, whilst a more arid climate is generally associated with relatively weak chemical weathering (Nesbitt and Young, 1982).

The relationship between climate and the degree of rock weathering has shown that higher rainfall corresponds to the increased loss of labile minerals, and higher CIA values in the resulting sediments (Basu, 1981; James et al., 1981; Suttner et al., 1981; Dutta and Suttner, 1986; Girty, 1991; White and Blum, 1995). Consistent rainfall will continuously flush a weathering profile with unsaturated fluids for hydrolysis, remove the products of ion exchange, and volumetrically more parent rock material will be subjected to decomposition over a given unit time. The CIA values of the studied sandstones vary from 75 to 82 (except 3 samples) and shales from 76 to 86. This suggests that the source rocks of these sedimentary rocks are subjected to strong chemical weathering and generated and deposited under a climatic regime that included significant rainfall. Therefore, the Jumara Dome rocks are affected by strong chemical weathering and formed under warm and humid climate conditions.

The bivariant ratio of polycrystalline quartz to feldspar plus rock fragments (Suttner and Dutta, 1986) has been used for interpreting the paleoclimate of Jumara Dome Sandstones. Figure 7A indicates a humid climate prevailing in the region. The paleoclimate simulations for the Jurassic and Lower Cretaceous show that India as a part of the Gondwanaland experienced humid to tropical climates (Thompson and Barron, 1981; Chatterjee and Hotton, 1986; Chandler et al., 1992).

The precipitation of huge carbonates during the Jurassic is also supportive of the fact that the area was witnessing a warm climate similar to that found in the tropics. A combination of low relief, hot humid climate and ample vegetation can produce quartz-rich detritus (Franzinelli and Potter, 1983). Low relief provides prolonged residence time of sediments, thereby increasing the duration of chemical weathering and

thus forming stable quartz in the sediments. The mineralogical data in the diagram of Weltje et al. (1998) fall in the No. 1 field which points in the sedimentation on a low relief and temperate sub-humid condition (Fig. 7B). Overall study suggests that such strong chemical weathering condition is inconformable with worldwide humid and warm climates during the Jurassic period (Thompson and Barron, 1981). This may be the result of non-steady-state weathering conditions where active tectonism and uplifting allow erosion of all soil horizons and rock surfaces (Nesbitt et al., 1997).
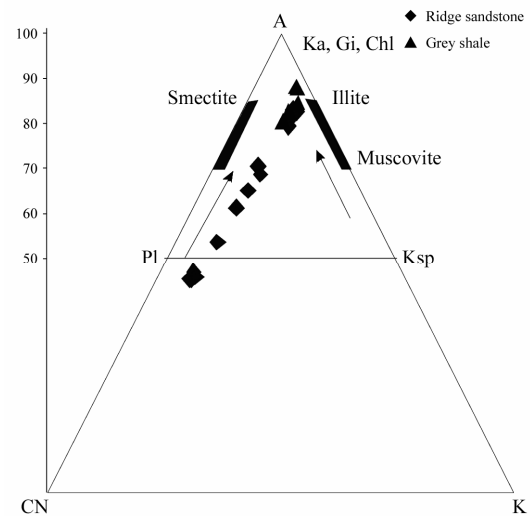
Fig. 6. A-CN-K (in molecular proportion) ternary plot (Nesbitt and Young, 1984) for the Jumara Dome sediments. Ka. Kaolinite; Gi. Gibbsite; Ch. Chlorite; Pl. plagioclase; Ksp. K-feldspar.

6.3 Provenance and tectonic setting

The studied sandstones are quartzarenitic and subarkosic in nature, which suggests interplay of pulses of rapid uplift of the source area and quick subsidence of the basin, followed by a period of quiescence within an overall transgressive-regressive cycle in a rift tectonic regime. The first-cycle quartz sand may have been supplied from a nearby quartz-rich source area. A unique combination of tropical climate, low relief, low rate of sedimentation and long residence on the beach is considered to produce mature and first-cycle quartzarenite (Suttner et al., 1981). The studied sandstone composition suggests that during basin unstability, sediments supplied from the source area were quickly buried and more or less retained the original composition except for modification of unstable constituents induced by chemical weathering, which has a greater capacity to alter sandstone composition (Basu, 1976; Franzinelli and Potter, 1983; Suttner and Dutta, 1986).
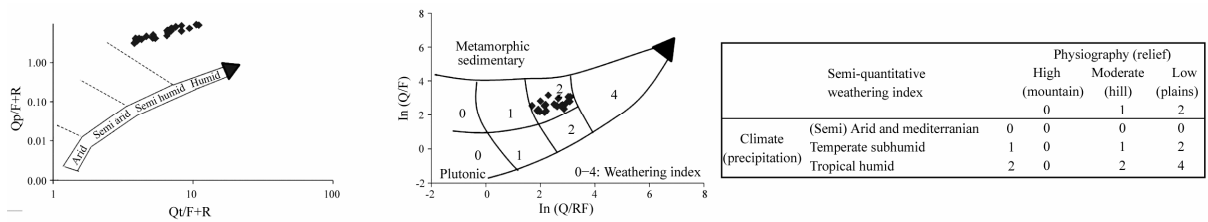
Fig. 7. A. Bivarent log/log plot for Ridge sandstone, Jumara Dome, Kachchh (according to Suttner and Dutta, 1986), B. log ratio plot after Weltje et al. (1998). Q=Quartz; F=Feldspar; RF=Rock fragments.

The plots of the Ridge sandstone on the Qt-F-L and Qm-F-Lt diagrams suggest that the detritus of the sandstones was derived from the granite-gneisses exhumed in the craton interior as well as low- to high-grade metamorphic supracrustal forming recycled orogen shedding quartz debris of the continental affinity into the basin. The Qp-Lv-Ls plot reveals the source in the rifted continental margin, collision suture and fold thrust belt. In the Qm-P-K diagram, the data lie in the continental block provenance reflecting the maturity of the sediments and the stability of the source area. This may have stemmed from a very long period of tectonic quiescence and mature geomorphology of the area. The provenance for the Ridge sandstone is believed to be weathered parts of the present day, the Aravalli range situated to the northeast and southeast of the basin and the Nagarparkar massif situated to the north and northwest of the basin. This is indicated by the sand dispersal pattern studied by various researchers (Balagopal and Srivastava, 1975; Dubey and Chatterjee, 1997, Ahmad and Bhat, 2006). The tectonics of the Aravalli-Delhi Folded Belt (ADFB) makes it collage of recycled orogen and basement uplift provenance. It is expected that sandstone detrital modes were derived from ADFB and would plot in a recycled orogen provenance. But most of the petrofacies Qt-F-L and Qm-F-Lt plot in the continental block provenance. False signature of continental block provenance may be the result of several factors, which have modified the original composition of the detritus in one way or another. The major controls on the detritus composition are exerted by paleoclimate, transport and diagenesis. Analysis of major elements was used to discriminate the tectonic setting of the sandstones studied by Schwab (1975), Bhatia (1983), Roser and Korsch (1986, 1988) and Armstrong-Altrin et al. (2004). It was suggested the use of the discriminate function diagram to understand the provenance for the feldspathic terrain. Figure 8 suggests that the sediments were derived mainly from mature polycyclic continental sedimentary rocks, followed by dominantly basaltic and less andesitic rocks. The studied sandstones and shales were derived from the recycled orogenic terrain (granite-gnessiss or quartzose sedimentary provenance source area).

SiO_2-K_2O/Na_2O ratio diagrams were plotted in accordance to Roser and Korsch (1986), suggesting that the studied sandstone/shale samples fall in the field of "passive tectonic margin" (Fig. 9). The petrographic and geochemical data strongly suggest that the studied sandstones/shales were deposited on a passive margin of a stable intracratonic basin. The ternary plot of Kroonenberg (1994) also favours a passive margin setting (Fig. 10).
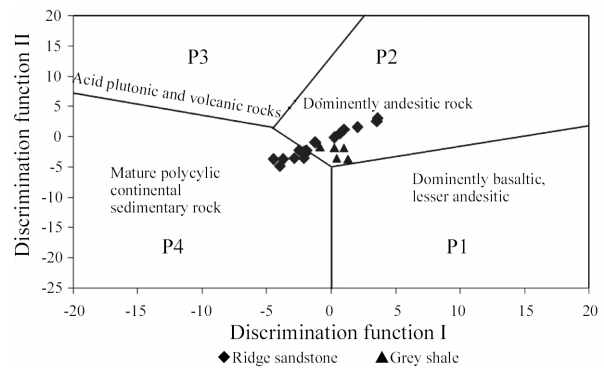
Fig. 8. Discrimination function diagram (Roser and Korsch, 1986).
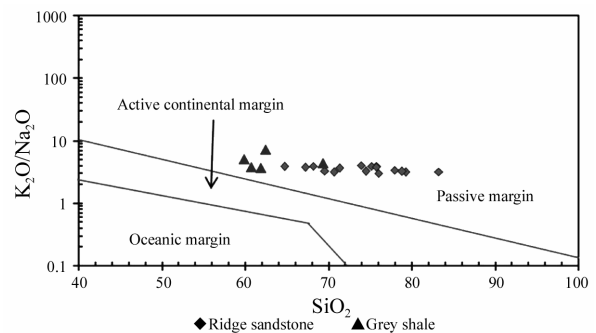
Fig. 9. Tectonic discrimination diagram for Jumara Dome sediments (Roser and Korsch, 1986).

Samples of Ridge sandstone and shale exhibit variable enrichment and depletion in their major and trace elements compared to PAAS (Post Archean Australian Shale). For a realistic comparison, average elemental abundances of both sandstones and shales are normalized to PAAS (Fig.11A, B). It is evident that Ridge sandstone possesses depleted values of all major oxides, and trace elements including LREE ex-

cept SiO$_2$ and CaO (slightly enriched), Zr (significantly enriched) and Y similarly compared to PAAS. This depletion appears to be due to quartz dilution effect and Zr enrichment may be attributed to the enriched Zr content in the source, this should have resulted in the enrichment of REE, too. Zircon enrichment in the sandstones also supports the inference that the sandstones may have been derived from a granitic source. But REE is also not probably depleted in the sandstones (Fig.11A). The average Si, Al, Ti, Rb, Nb, Cr, Ni and LREE contents of the shales are more or less the same as those of PAAS (Fig.11B). However, the average values of Fe, Mg, Na, K, Ba and CO are slightly depleted compared to those of PAAS. Zr is enriched in the shales like in the sandstones. The analogous contents of Si, Al, Ti, LREE and TTE in the shales to PAAS with slightly depleted values of other elements ascribe a PAAS-like source (granitic gneiss and minor mafics) to the rocks of the present study.
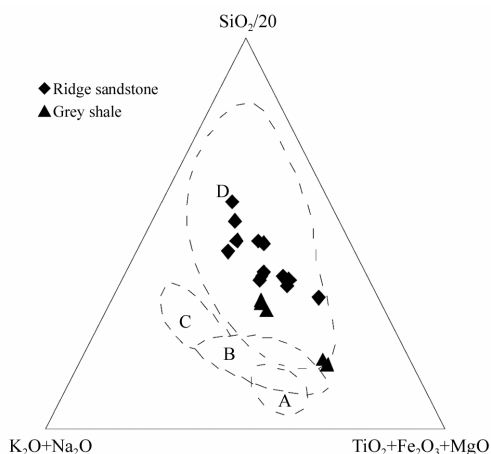
Fig. 10. Plot of the major elements composition of the Jumara Dome sediments on the tectonic setting discrimination diagram of Kroonenberg (1994).

7 Discussion

The Jumara Dome sediments were derived from a variety of source rocks comprising granitic batholiths/igneous plutons, magmatic- arc granite-gneisses, pegmatite or schist, metaquartzite, quartz vein, etc. The plots of Ridge Sandstone on the Qt-F-L and Qm-F-Lt diagrams suggest that the detritus of the sandstones was derived from the granite-gneisses exhumed in the craton interior as well as low- to high-grade metamorphic supracrustal forming recycled orogen shedding quartz debris of the continental affinity into the basin. The sediments were mainly deposited under the rifted basin condition as evidenced by the plot on the Qp-Lv-Ls diagram. The Qm-P-K diagram suggests the maturity and stability of the source region. The A-CN-K suggests that the rocks would be derived from a source more or less similar to diorite source. Moreover, the data on the

CaO-Na$_2$O-K$_2$O diagram (after Bhatia, 1983) cluster within the granitic field. The discrimination diagram of Roser and Korsch (1986) suggests that the studied rocks were deposited in passive margin settings. The heavy mineral suites like well rounded grains of tourmaline, biotite rutile and zircon were perhaps derived from the Aravalli metasediments. The garnet, staurolite and epidote grains originating from the Aravalli pelitic metasediments which have been described to attain high rank metamorphism at places found in the Ridge sandstone reflect their sources in the mixed provenance, such as that being believed to represent the eroded and weathered parts of the present day, the Aravalli range is situated to the east and northeast of the basin and the Nagarparkar massif is situated to the north and northwest (Dubey and Chatterjee, 1997). Various chemical indices such as CIA, ICW, PIA and ICV suggest that the source rocks of the Jumara Dome sediments have suffered moderate to intense chemical weathering. The rocks were formed from the sediments characterized by recycled input or intense weathering of the first cycle sediments. The study further suggests that the Jumara Dome sediments are compositionally mature as they possess along with the first cycle sediments deposited in a tectonically quiescent or cratonic environment.

8 Conclusions

The studied rocks of Jumara Dome sediments occupied by the subarkose, arkose, litharenite and wacke fields. Due to gradational behaviour of the major and trace elements in these two rocky types from the Ridge sandstone and Grey shale, they have been considered as a single sequence irrespective of the stratigraphy where they have been defined as different members. The petrofacies analysis of the sandstones suggests continental block provenances with source on a stable craton which has been recognized as the Aravalli Craton. The continental block provenance that supplied detritus to the Kachchh rift was deeply weathered. The fault bounded basement uplifts along incipient rift belts within the continental block are known to shed arkosic sands into adjacent linear troughs, but quartz-rich detritus was deposited into the Kachchh rift because of warm and humid climate, low relief and long residence time in soil. The higher average value of CIA reveals moderate- to high-degree chemical weathering possibly under warm and humid climatic conditions. The ICV values and major and trace elements signatures indicate that sedimentation took place in a passive margin tectonic setting. The study reveals that the basin received the mixture of debris derived from a proximal source in the initial stage of sedimentation and distal source during the later stage of basin development. Integrated analysis of petrographic and geochemical characteristics coupled
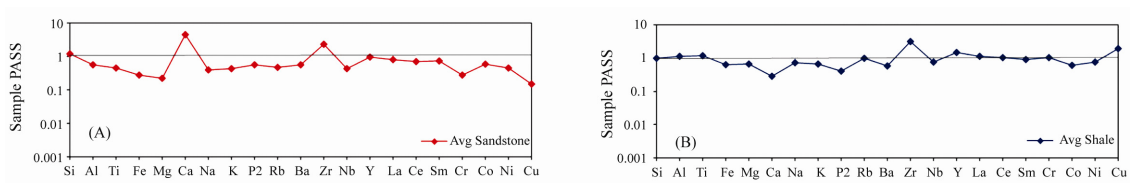
Fig. 11. Average elemental abundances of both sandstones and shales are normalized to PAAS.

Plate I: A. Field photograph showing large scale planar cross-bedding; B. trough cross-bedding; C. lamination.
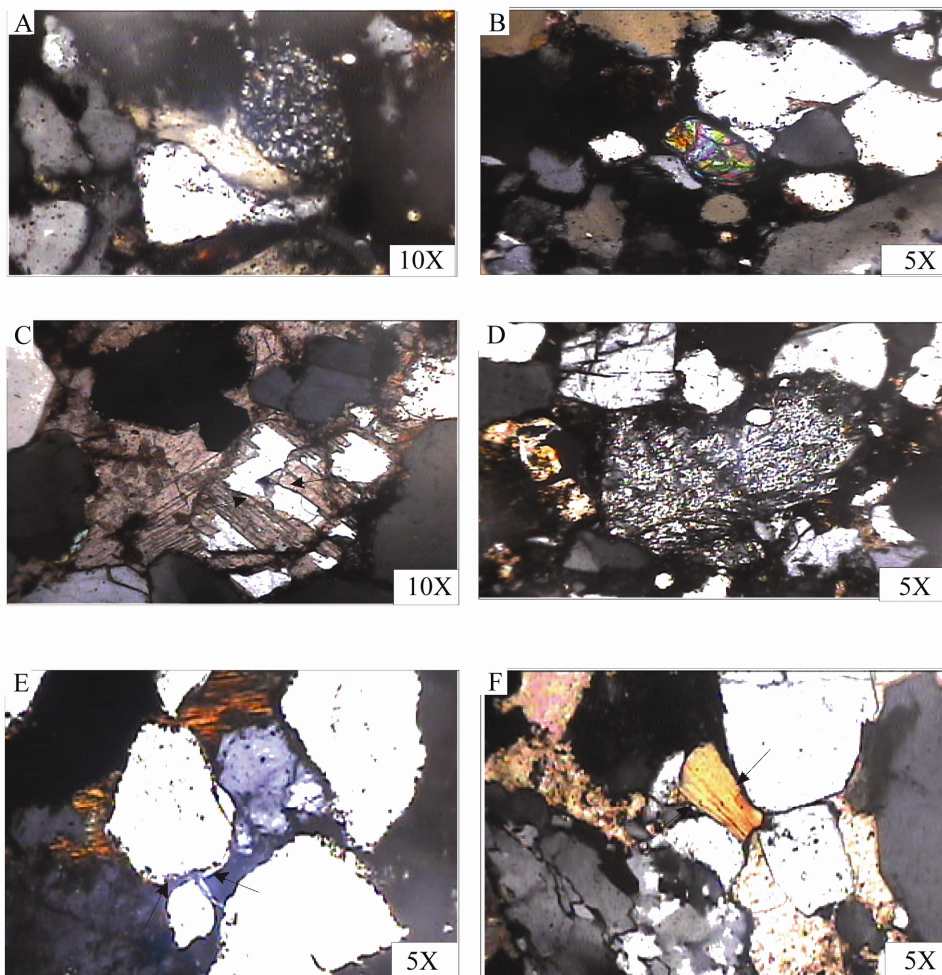
Plate II: A. Photomicrograph showing chert grain; B. zircon grain; C. quartz grain corroded by carbonate cement; D. iron cement corroded feldspar grain; E. quartz overgrowth; F. kaolinite.

with paleocurrent direction of the Jurassic sandstones/shales of the Kachchh Basin suggests that sand detritus was mostly derived from the Aravalli range situated to the northeast, east and southeast of the basin and from the Nagar parker massif situated to north and northwest of the basin. The first phase of diagenesis consisted of mechanical compaction and precipitation of small amounts of quartz cement. The second phase in which pore spaces were almost coupled obliterated solutions in the fresh water phreatic zone. However, secondary porosity was generated by dissolution and leaching of feldspar grains, calcite and iron oxide cements. Once again both porosity and permeability were reduced at a later date by the deposition of authegenic kaolinite in the secondary pore spaces of a sandstone unit.

References

Ahmad A.H.M. and Bhat G.M. (2006) Petrofacies, provenance and diagenesis of the Dhosa Sandstone Member (Chari Formation) at Ler, Kachchh sub-basin, Western India [J]. *Journal of Asian Earth Sciences*. **27**, 857–872.

Armstrong-Altrin J.S., Lee Y.I., Verma S.P., and Ramasamy S. (2004) Geochemistry of sandstone from upper miocene Kudankulam Formation, southern India: Implication for provenance, weathering and tectonic setting [J]. *Journal of Sedimentary Research*. **74**, 285–297.

Balagopal A.T. and Srivastava V. K. (1975) A study of the paleocurrent and the provenances of the Jurassic rocks of Central Kutch, Gujarat state [J]. *Indian Journal of Earth Sciences*. **2**, 62–76.

Bardan S. and Datta K. (1987) Biostratigraphy of Jurassic Chari Formation, a study in Keera dome, Kutch, Gujarat [J]. *Journal of the Geological Society of India*. **30**, 121–131.

Basu A. (1976) Petrology of Holocene fluvial sand derived from plutonic source rocks: Implication to paleoclimatic interpretations [J]. *Journal of Sedimentary Petrology*. **40**, 694–709.

Basu A. (1981) Weathering before the advent of land plants evidence from unaltered detrital K-feldspar in Cambrian-Ordovician arenites [J]. *Geology*. **9**, 132–133.

Basu A., Young S.W., Suttner L.J., James W.C., and Mack G.H. (1975) Re-evaluation of the use of undulatory extinction and polycrystallinity in detrital quartz for provenance interpretation [J]. *Journal of Sedimentary Petrology*. **45**, 873–882.

Bhatia M.R. (1983) Plate tectonics and geochemical composition of sandstones [J]. *Journal of Geology*. **91**, 611–627.

Bhatia M.R. and Crook K.A.W. (1986) Trace elements characteristics of greywacke and tectonic setting discrimination of sedimentary basins [J]. *Contributions to Mineralogy and Petrology*. **92**, 181–193.

Biswas S.K. (1987) Regional tectonic framework, structure and evolution of the western marginal basins of India [J]. *Tectonophy*. **135**, 307–327.

Chandler M.A., Rind D., and Ruedy R. (1992) Pangean climate during early Jurassic GCMS simulations and sedimentary record of Paleoclimate [J]. *Bulletin of the Geological Society of America*. **104**, 543–559.

Chatterjee S. and Hotton N. (1986) The Paleoposition of India [J]. *Journal of Southeast Asia Earth Sciences*. **1**, 145–189.

Condie K.C. (1993) Chemical composition and evolution of the upper continental crust: Contrasting results from surface samples and shales [J]. *Chemical Geology*. **104**, 1–37.

Cox R., Lowe D.R., and Cullers R.D. (1995) The influence of sediment recycling and basement composition on evolution of mudrock chemistry in the southwestern United States [J]. *Geochimica et Cosmochimica Acta*. **59**, 2919–2940.

Crook K.A.W. (1974) Lithogenesis and geotectonics: The significance of compositional variation in flysch arenites (greywackes) [J]. *Society of Economic Paleontology and Mineralogist*. **19**. 304–310.

Cullers R.L. (1988) Mineralogy and chemical changes of soil and stream sediments formed by intense weathering of the Danburg granite, Georgia, U.S.A. [J]. *Lithos*. **21**, 301–314.

Cullers R.L. (2000) The geochemistry of shales, siltstones and sandstones of Pennsylvanian-Permian age, Colorado, U.S.A.: Implications for provenance and metamorphic studies [J]. *Lithosratigraphy*. **51**, 305–327.

Dickinson W.R., and Suczek C.A. (1979) Plate-tectonics and sandstones composition [J]. *American Association of Petroleum Geologist Bulletin*. **63**, 2164–2182.

Dickinson W.R., Beard L.S., Brakenridge G.R., Erjavec J.L., Ferguson R.C., Inman K.F., Knepp R.A., Lindberg F.A., and Ryberg P.T. (1983) Provenance of North American Phanerozoic sandstones in relation to tectonic setting [J]. *Geological Society of America Bulletin*. **94**, 222–235.

Dickinson W.R. (1985) *Interpreting Relations from Detrital Modes of Sandstone, Provenance of Arenites* (ed. Zuffa G.G.) [C]. pp.333–361. Dordrecht-Boston-Lancaster.

Dubey N. and Chatterjee B.K. (1997) Sandstones of Mesozoic Kachchh Basins: Their provenance and basinal evolution, India [J]. *Journal of Petroleum Geology*. **6**, 55–58.

Dutta P. and Suttner L. (1986) Alluvial sandstone composition and paleoclimate authigenic mineralogy [J]. *Journal of Sedimentary Petrology*. **56**, 346–358.

Fedo C.M., Young G.M., Nesbitt H.W., and Hanchar J.M. (1997) Potassic and sodic metasomatism in the southern Province of the Canadian Shield: Evidence from the Paleoproterozoic Serpent Formation, Huronian Supergroup, Canada [J]. *Precambrian Research*. **84**, 17–36.

Franzinelli E. and Potter P.E. (1983) Petrology, chemistry and texture of modern river sands, Amazon River system [J]. *Journal of Geology*. **91**, 23–39.

Fursich F.T., Oschmann W., Jaitely A.K., and Singh I.B. (1991) Faunal response to transgressive and regressive cycles–Examples from Jurassic of Western India [J]. *Palaeogeography, Palaeoclimatology, Palaeoecology*. **85**, 149–159.

Girty G.H. (1991) A note on the composition of plutonic clastic sand produced in ifferent climatic belts (short notes) [J]. *Journal of Sedimentary Petrology*. **61**, 428–433.

James W., Mack G., and Suttner L. (1981) Relative alteration of microcline and sodic plagioclase in semi arid and humid climates [J]. *Journal of*

Sedimentary Research. **51**, 151–164.

Koshal V.N. (1984) Differentiation of Rhaetic sediments in the subsurface of Kutch based on Palynofossils [J]. *Petroleum Asia Journal*. **7**, 102–105.

Kroonenberg S.B. (1994) Effect of provenance, sorting and weathering on the geochemistry of fluvial sand from different tectonic and climate environments: Proceedings of the 29th International Geological Congress [Z]. pp.69–81.

McBride E.F. (1985) Diagenetic processes that effects provenance determination in *Sandstone Provenance of Arenites* (ed. Zuffa G.G.) [Z]. pp.95–114. Reidel, Dordrecht-Boston-Lancaster.

McLennan S.M. and Taylor S.R. (1991) Sedimentary rocks and crustal evolution, tectonic setting and secular trends [J]. *Journal of Geology*. **99**, 1–21.

McLennan S.M., Hemming S., McDaniel D.K., and Hanson G.N. (1993) Geochemical approaches to sedimentation, provenance and tectonics [J]. *Geological Society of America Bulletin*. **284**, 21–40.

Nesbitt H.W. and Young G.M. (1982) Early Proterozoic Climates and plate motion Inferred from major element chemistry of lutites [J]. *Nature*. **299**, 715–717.

Nesbitt H.W. and Young G.M. (1984) Prediction of some weathering trend of plutonic and volcanic rocks based on thermodynamic and kinetic consideration [J]. *Geochimica et Cosmochimica Acta*. **48**, 1523–1534.

Nesbitt H.W., Fedo C.M., and Young G.M. (1997) Quartz and feldspar stability, steady and non-steady-state weathering and pedogenesis of siliciclastics sands and muds [J]. *Journal of Geology*. **105**, 173–191.

Norton I.D. and Sclater J.G. (1979) A model for the evolution of the Indian Ocean and the breakup of Gondwanaland [J]. *Journal of Geological Research*. **84**, 6803–6830.

Roser B.P. and Korsch R.J. (1986) Determination of tectonic setting of sandstone-mudstone suites using SiO_2 content and K_2O/Na_2O ratio [J]. *Journal of Geology*. **94**, 635–650.

Roser B.P. and Korsch R.J. (1988) Provenance signatures of sandstone-mudstone suites determined using discrimination function analysis of major-element data [J]. *Chemical Geology*. **67**, 119–139.

Schwab F.L. (1975) Framework mineralogy and chemical composition of continental margin-type sandstone [J]. *Journal of Geology*. **34**, 331–340.

Suttner L.J., Basu A., and Mack G.H. (1981) Climate and the origin of quartz-arenites [J]. *Journal of Sedimentary Petrology*. **51**, 1235–1246.

Suttner L.J. and Dutta P.K. (1986) Alluvial sandstones composition and paleoclimate, I, framework mineralogy [J]. *Journal of Sedimentary Petrology*. **56**, 329–345.

Taylor S.R. and McLennan S.M. (1985) *The Continental Crust: Its Composition and Evolution: An Examination of the Geochemical Record Preserved in Sedimentary Rocks* [M]. pp.312. Blackwell Science, Oxford.

Thompson S.L. and Barron E.J. (1981) Comparison of Cretaceous and present earth albedos: Implication for the causes of Paleoclimates [J]. *Journal of Geology*. **89**, 143–167.

Walker R.G. (1984) *Shelf and Shallow Marine Sands* (ed. Walker R.G.) [M]. pp.141–170. Facies Models, *Geoscience Canada Reprint Ser*. **1**.

Weltje G.J., Meijer X.D., and Doer P.L. (1998) Stratigraphic inversion of siliciclastic basin fills: A note on the distinction between supply signals resulting from tectonic and climate forcing [J]. *Basin Research*. **10**, 129–153.

Weltje G.J. and Eynatten H.V. (2004) Quantitive provenance analysis of sediments: Review and outlook [J]. *Sedimentary Geology*. **171**, 1–11.

White A. and Blum A. (1995) Effects of climate on chemical weathering in water shed [J]. *Geochimica et Cosmochimica Acta*. **59**, 1729–1747.